Accepted Manuscript

Title: Localized stress percolation through dry masonry walls. Part ii modelling

Authors: Davide Bigoni, Giovanni Noselli

PII: S0997-7538(09)00130-2

DOI: 10.1016/j.euromechsol.2009.10.013

Reference: EJMSOL 2565

To appear in: *European Journal of Mechanics / A Solids*

Received Date: 6 July 2009

Revised Date: 15October2009

Accepted Date: 21 October 2009

Please cite this article as: Bigoni, D., Noselli, G. Localized stress percolation through dry masonry walls. Part ii modelling, European Journal of Mechanics / A Solids (2009), doi: 10.1016/j.euromechsol.2009.10.013

LOCALIZED STRESS PERCOLATION THROUGH DRY MASONRY WALLS. PART II MODELLING

DAVIDE BIGONI and **GIOVANNI NOSELLI**

Dipartimento di Ingegneria Meccanica e Strutturale, Università di Trento, Via Mesiano 77 – 38050 Povo, Trento, Italia[1]

The highly localized stress distribution found within dry masonry walls through transmission photoelasticity in Part I of this article is explained both proposing a micromechanical model (based on a form of random cascade transmission of forces between bricks, which includes random coalescence additionally to random branching) and applying a phenomenological description (based on the extreme orthotropy of the equivalent homogeneous material).

Key words: Photoelasticity, masonry, granular materials, localized stress paths

1. Introduction

Transmission photoelasticity has been shown in Part I of this article to reveal the highly inhomogeneous stress distribution within dry masonry walls, where 'unloading islands' emerge in a narrow 'stress stream'. The key to the interpretation of these experimental results is randomness (but constrained within the regular scheme imposed by the masonry) of contacts between bricks and 'overall' material orthotropy with high-contrast in elastic moduli. Accordingly, two alternatives are proposed to *fully explain* experiments presented in Part I, namely, (i.) the micromechanical model –where the masonry is treated as an elastic structure with unilateral 'orderly random' contacts, to generate a form of random cascade of vertical forces, where 'random coalescence' may occur in addition to the usual rule of random branching– and (ii.) the continuum model –where the masonry behaves as a strongly orthotropic material close to the elliptic border and reveals stress localization following concepts proposed by Everstine and Pipkin (1971) and Bigoni and Capuani (2002; 2005).

Although they both successfully explain our experimental results, the micromechanical approach and the continuum model have limitations, in the sense that the former is a simple approach tailored on our experimental setting (so that it cannot be immediately generalized to cover complex stress situations), while the latter approach is general, though does not reproduce the diversity of the stress states within masonries (the two approaches could be combined, but

[1]*E-mail*: bigoni@ing.unitn.it, giovanni.noselli@ing.unitn.it; *Website*: http://www.ing.unitn.it/~bigoni/

this falls beyond the scope of the present article).

2. A resumé of experimental results

We refer to the experiments reported in Figs. 1 and 2, together with those reported in Part I of this article to highlight: (i.) the highly localized nature of (almost vertical) stress percolation within the masonry and (ii.) the fact that forces are almost vertically transmitted at random contacts between bricks.

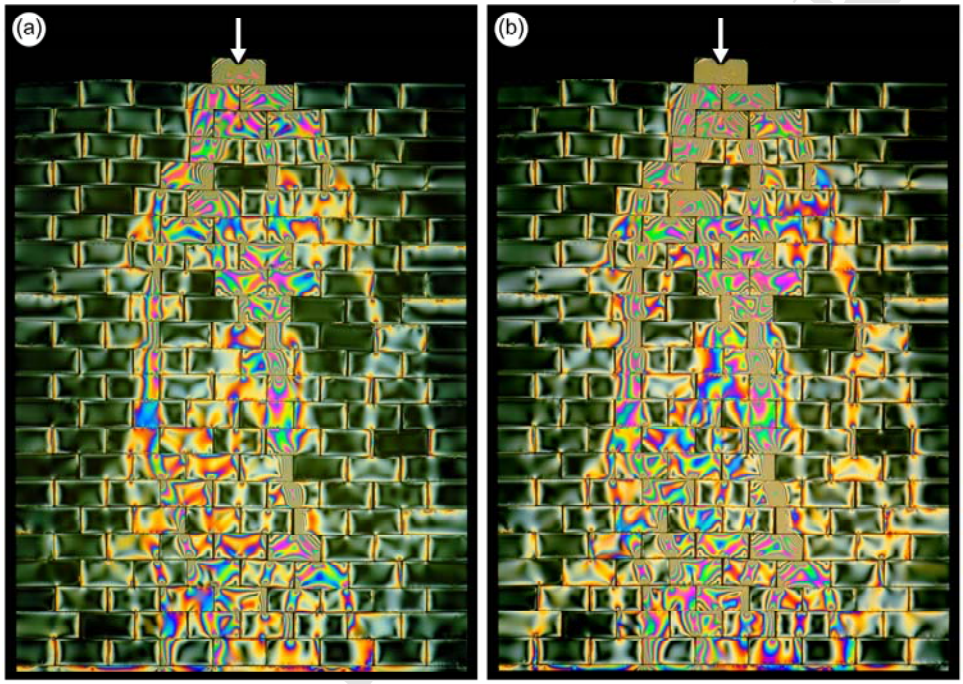

Fig. 1 – Photoelastic fringes of a model of dry masonry with thin vertical joints detected with a circular transmission polariscope at white light. (a) low vertical load (400 N); (b) high vertical load (800 N). Note the unloaded brick three courses below the applied vertical load (denoted with a white arrow).

A quantification of these forces has been proposed in Fig. 2 (which is the same photo reported in Fig. 2b of the Part I of this article), through comparison with the elastic solution of a disk subject to two equal and opposite forces (the material used is PSM-9, for which the fringe constant is known to be 10.5 kPa/fringe/m). The stress state in the disk is very similar to that obtained with f.e. simulations when the force is applied at the centre of the brick, so that the use of the analytical solution for the disk permits a fast and enough accurate treatment of the images.

The quantification of force percolation shown in Fig. 2 reveals that there is little diffusion of the load through the masonry, so that the 125 N plus 70 N force near the load application becomes75 N plus 75 N plus 45 N in the tree neighbor bricks near the bottom of the sample.

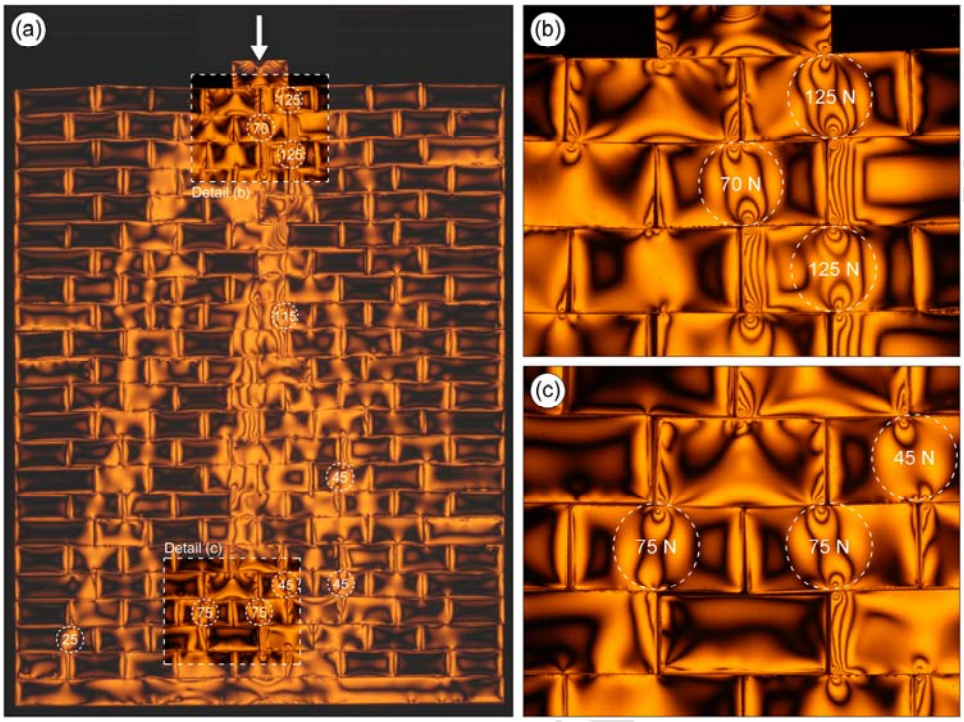

Fig. 2 – Photoelastic fringes of a model of dry masonry with thin vertical joints detected with a linear transmission polariscope equipped with sodium vapor lamp (axes at 45° with respect to the vertical) at an applied load of 250 N, denoted with a white arrow. Forces have been quantified through comparison with the solution of an elastic disk subject to two opposite forces. (a) is Fig. 2b of part I of this article. Details are reported in parts (b) and (c).

To fully appreciate the strong, qualitative difference between results reported in Figs. 1 and 2 and those pertaining to a model of identical dimension, *but homogeneous*, we report in Fig. 3 results pertaining a 72 mm × 88 mm × 6 mm rectangular plate of PSM-9 material, loaded in the same way as for the masonry models, namely, with a vertical force applied on a 8 mm × 4 mm × 6 mm punch (also made of PSM-9). The photo reported in Fig. 3, has been taken with the circular polariscope at 500 N vertical load, has been split into two parts and interpolated with the analytical solution for a uniform loading on a finite area of a semi-infinite elastic plate [which is derived below, eqn. (2), see also Johnson, 1985]. This solution can be derived from the problem of a concentrated force F orthogonal to the otherwise free surface of an elastic half space, the so-called 'Flamant solution', where only the radial stress is different from zero and is given by

$$\sigma_r(r,\vartheta) = -\frac{2F}{\pi}\cdot\frac{\cos\vartheta}{r}, \qquad (1)$$

where r is the radial distance between the vertical force and the point under consideration in the elastic half space, singled out by the angular coordinate ϑ, taken null when the point lies on the vertical line of the loading force.

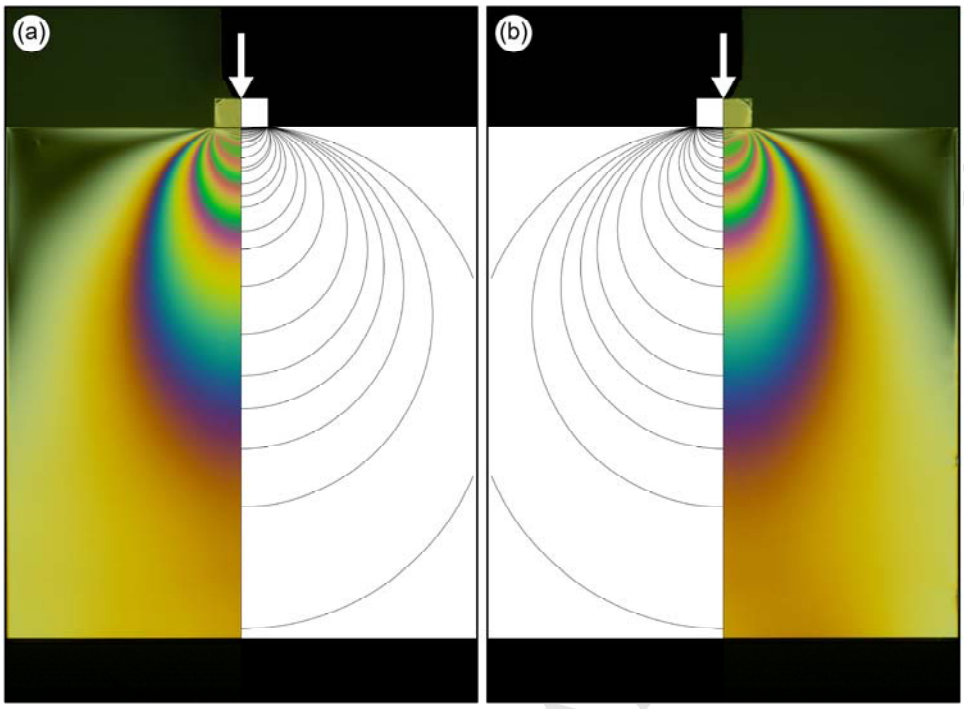

Fig. 3 – A uniform rectangular plate loaded on a small portion of its edge through a 500 N vertical force. Isochromatic fringes detected with a circular transmission polariscope at white light and compared to the analytical solution for an elastic homogeneous isotropic half space, loaded on a portion of its boundary, eqn. (2).

The stress state induced in the half space when a uniform load p is applied on a segment of length $2b$ is obtained in Cartesian coordinates through integration of eqn. (1) as

$$\sigma_{11}(x_1,x_2)=-\frac{2p}{\pi}\int_{-b}^{b}\frac{(x_1-\xi)^2 x_2}{\left((x_1-\xi)^2+x_2^2\right)^2}d\xi,$$

$$\sigma_{22}(x_1,x_2)=-\frac{2p}{\pi}\int_{-b}^{b}\frac{x_2^3}{\left[(x_1-\xi)^2+x_2^2\right]^2}d\xi, \qquad (2)$$

$$\sigma_{12}(x_1,x_2)=-\frac{2p}{\pi}\int_{-b}^{b}\frac{(x_1-\xi)x_2^2}{\left[(x_1-\xi)^2+x_2^2\right]^2}d\xi,$$

where x_1 and x_2 are respectively the horizontal and the vertical axes of a coordinate system centered at the middle of the uniformly loaded segment [$-b$, b].

Note that, although the stress field (2) is referred to a *semi-infinite* elastic medium, the comparison with the experiment reported in Fig. 3 and referred to a *finite* rectangular plate is very satisfactory. This is related to the fact that the loading punch is small when compared to the dimensions of the plate.

A comparison between Fig. 3 and the figures pertaining to the masonry models (Figs. 1 and

2, see also Part I of this article) reveals that the stress state within the masonry models deeply differs from the elastic, *isotropic* and homogeneous solution. This situation has been noted in somewhat similar experiments by Da Silva and Rajchenbach (2000). Their conclusion is that the experiments do not fit both elasticity and plasticity models, rather, they show diffusive patterns. Although we do not disprove their conclusions (rather we agree on several points), we suggest here an interpretation not involving any diffusion. In particular, we point out that experimental results on masonry models can be successfully interpreted in two alternative ways, namely, *either as the response of a highly inhomogeneous material composed by a regular –though discontinuous– structure, or as the response of a homogeneous elastic, but strongly orthotropic, material*. The former approach is based on micromechanical considerations, while a macroscopic modelling in terms of an equivalent homogeneous material is pursued following the latter approach. We explain both approaches below.

3. Interpretation of experimental results

There are two ways to explain the obtained experimental results: one is the micromechanical approach, in which the masonry is modelled as a discrete structure, where bricks are randomly in contact at their vertices; another is the continuum mechanics approach, in which the material is modelled as a continuous homogeneous material, characterized by an extreme orthotropy. Both approaches can be successfully developed as follows.

3.1. Micromechanics: masonry as a discrete structure with random contacts between bricks

The bricks have been found to be randomly in contact at their vertices, so that a simple micromechanical model of our masonries can be obtained as follows (explained with reference to the case of null vertical joints, while thick vertical joints are treated in Appendix A):

i.) our physical models are loaded vertically and experiments show that friction does not play an important role. Friction is therefore neglected in the mathematical model, so that it is assumed that forces percolate only vertically through the masonry;

ii.) since experiments show that forces are localized near the brick vertices, we assume that every brick is loaded at its upper edge by three compressive vertical forces, applied at the centre of the edge and at the vertices (F_1, F_2 and F_3 in Fig. 4b). Moreover, the contact points at the lower edge of a brick are always two, to be randomly chosen between three possibilities (labeled 1, 2 and 3 in Fig. 4b);

iii.) equilibrium of the brick and unilaterality of the contacts at the lower edge of it determine the vertical reaction forces (R_1, R_2 and R_3 in Fig. 4b), which become the vertical forces at the upper edges of the bricks at the lower course.

More in detail, the load transmission mechanism 1 involves two reaction forces applied at the lower corners of the brick, determined as

$$R_1 = F_1 + \frac{F_2}{2}, \quad R_2 = 0, \quad R_3 = F_3 + \frac{F_2}{2}. \tag{3}$$

The load transmission mechanism 2 (3) involves a reaction force applied at the central point of the lower edge of the brick, plus a reaction force applied at the left (right) corner or a reaction force applied at the right (left) corner, depending on the satisfaction of the unilateral constraint that no tensile forces are transmitted throughout the masonry. The reaction forces are thus determined as

$$R_1 = \langle F_1 - F_3 \rangle, \quad R_2 = F_1 + F_2 + F_3 - \langle F_1 - F_3 \rangle - \langle F_3 - F_1 \rangle, \quad R_3 = \langle F_3 - F_1 \rangle, \tag{4}$$

where $\langle\ \rangle$ denotes the Macaulay brackets defined for all $\alpha \in \mathbb{R}$ as $\langle \alpha \rangle = (|\alpha| + \alpha)/2$.

The algorithm to determine a force percolation within a masonry works as follows. For a given masonry geometry, first, the load mechanisms between the bricks are randomly generated (employing a discrete probability density function) selecting between the three possibilities listed in Fig. 4b and, second, the forces and the contact points are obtained by employing eqns. (3) or (4). The proposed algorithm works in such a way that all equilibrium conditions (including rotational equilibrium) and unilateral constraints are automatically satisfied.

It is clear that *the structure is statically determinate and there is a great (although finite) number of force distributions (but all constrained to lie within a certain 'limit' geometry and to possess a certain 'regularity') to equilibrate a given vertical load.* [2] Moreover, the obtained force distribution is a type of random cascade, in which some additional rules have to be enforced, so that random branching (Fig. 4c) is also accompanied by *random coalescence*, occurring when two or three vertical forces applied at the upper edge of a brick coalesce into one or two (Fig. 4d).

An example of the above procedure for determining a force distribution in a masonry is shown in Fig. 4a, where darker bricks are more loaded than lighter. This stress distribution has been generated to mimic the experiment shown in Fig. 1. After the load percolation through the

[2] Since force distributions are always possible and these will ensure equilibrium for applied vertical load distribution of arbitrary intensity, a collapse load will not be predicted for applied vertical loads, a conclusion consistent with limit analysis, where compressive strength is usually taken to be infinite (Heyman, 1966).

masonry has been generated with the above-explained algorithm, the stress state within the bricks and the relative simulation of photoelastic fringe patterns (corresponding to in-plane principal stress contours) has been evaluated (with ABAQUS-Standard, Ver. 6.7-1, Hibbitt, Karlsson & Sorensen Inc., employing 4-nodes bilinear elements CPS4), as in Fig. 5 of Part I, and reported in Fig. 5.

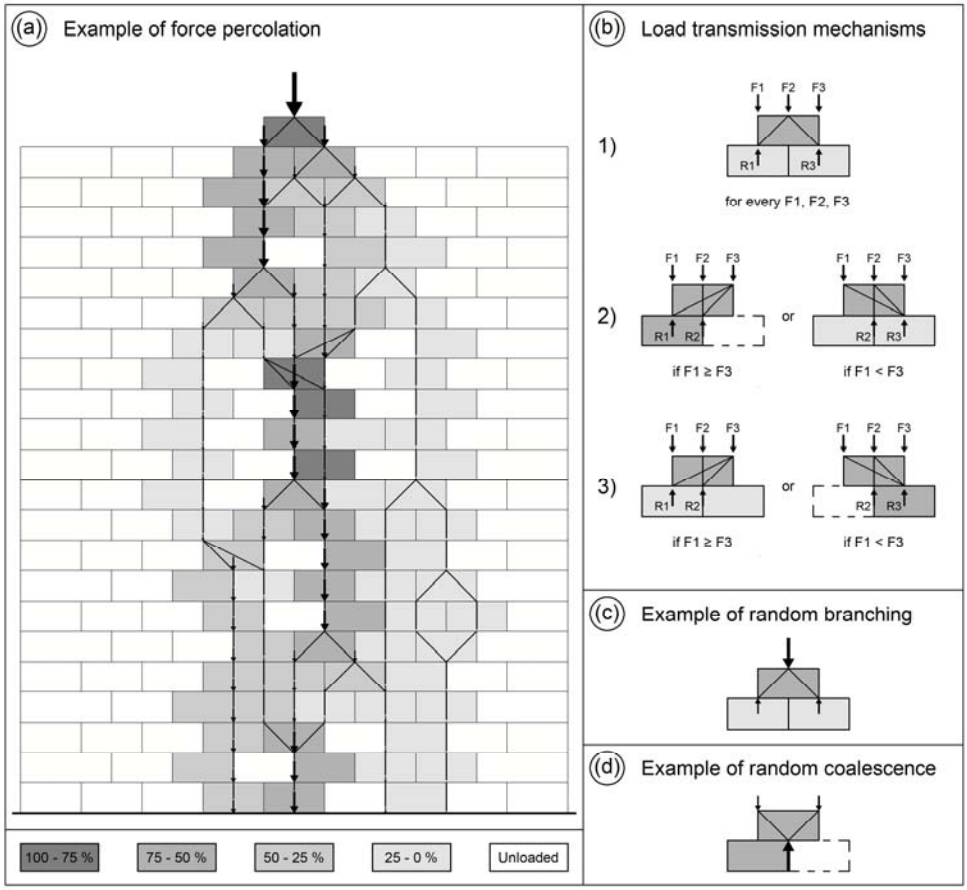

Fig. 4 – Model of a masonry as a discrete system with a form of random cascade vertical force transmission, where 'random coalescence' is possible, in addition to random branching. An example of force diffusion tree similar to results reported in Fig. 1 is given in (a), where the darker is the color, the higher is the force transmitted (white bricks are unloaded, see the scale reported in the lower part of the figure, where the transmitted percent of vertical load has been reported). Force transmission mechanisms are given respectively in part (b), while examples of random force branching and coalescence are presented in parts (c) and (d), respectively.

Due to the assumed randomness of the contacts, from a practical point of view only 'some' of the *possible* stress distributions can be investigated with the proposed model; however, the obtained *diversity* of the possible stress distributions reproduces our experimental results.

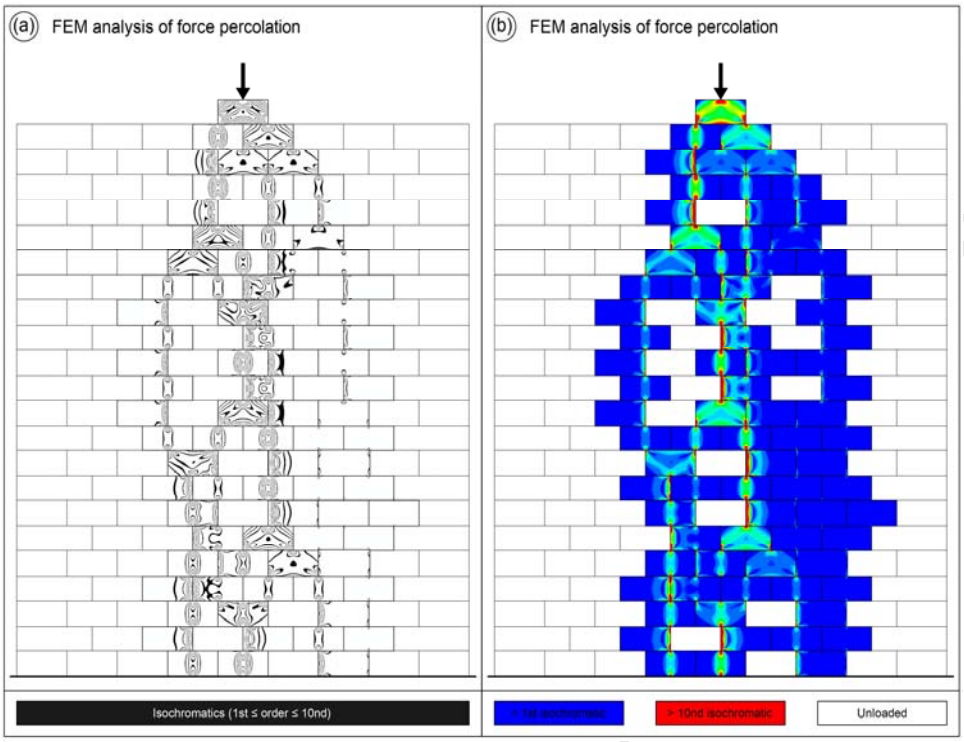

Fig. 5 – Simulation of isochromatics for the masonry loaded through the force percolation reported in Fig. 4a is analyzed with linear elastic f.e. Monochromatic [part (a)] and colored [part (b)] contours denote calculated in-plane principal stress difference, corresponding to photoelastic fringes.

The proposed model shares some similarity with the so-called '*q*-model' proposed by Liu et al. (1995) (see also Coppersmith et al., 1996), in which the percolation of vertical forces through a granular system is analyzed assuming that the vertical forces are randomly distributed at n contact points, so that for $n = 2$, a unit force is split into a force q and another force $1–q$. Although rotational equilibrium is violated and horizontal forces are neglected (Socolar, 1998), the *q*-method allows successful predictions of so-called 'force chains' in random distributions of photoelastic disks. However, the *q*-model does not provide information on the stress distribution within the elements, while our method, in which both equilibrium and unilaterality of contact are preserved, allows determination of stresses even inside the bricks.

3.2. Masonry as a continuous material with extreme orthotropy

In a macroscopic modelling, the highly inhomogeneous structure of the masonry models is 'viewed at a distance' from which inhomogeneity can be disregarded, so that the response of an uniform equivalent continuum is considered. In these conditions, the diversity of the possible stress percolations in nominally identical structures is necessarily lost, since these become in a sense identical when 'viewed at a sufficient distance' and they appear as manifestations of the

same localized stress distribution.

Since prior to vertical loading bricks are set in contact only under the (evidently small) effect of gravity, the vertical joints are unable to sustain any (normal or shearing) traction, while the horizontal joints cannot support shearing stress, but they can carry orthogonal compressive forces. In these conditions and due to the specific geometry of the masonry, the material becomes equivalent to an orthortropic homogeneous material, with a high contrast between stiffness moduli.[3]

The solution for a concentrated force F orthogonal to the otherwise free surface of an elastic orthotropic half space (with orthotropy x_1–x_2 axes aligned parallel and orthogonal to the free surface) has been found by Lekhnitskii (1981). With reference to an elastic material loaded in plane stress (as is the case of our masonry models), the constitutive equations can be written in inverse

$$\varepsilon_{11} = \frac{1}{E_1}\left(\sigma_{11} - \nu_{12}\sigma_{22}\right), \qquad \varepsilon_{22} = \frac{1}{E_2}\left(\sigma_{22} - \nu_{21}\sigma_{11}\right), \qquad \varepsilon_{12} = \frac{1}{2\,\mu_{12}}\sigma_{12}, \tag{5}$$

and direct form

$$\sigma_{11} = \frac{E_1}{1-\nu_{12}\nu_{21}}\left(\varepsilon_{11} + \nu_{21}\varepsilon_{22}\right), \quad \sigma_{22} = \frac{E_2}{1-\nu_{12}\nu_{21}}\left(\varepsilon_{22} + \nu_{12}\varepsilon_{11}\right), \quad \sigma_{12} = 2\,\mu_{12}\,\varepsilon_{12}, \tag{6}$$

where E_1 and E_2 are the two Young moduli in the directions 1 and 2 respectively, μ_{12} is the shear modulus, while ν_{12} and ν_{21} play a role similar to the Poisson coefficient of isotropic elasticity.

The solution for the concentrated force, where only the radial stress is different from zero and defining ϑ as the angle taken from the vertical line of the load F, is expressed by

$$\sigma_r(r,\vartheta) = -\frac{F}{\pi}\cdot\frac{\cos\vartheta}{r}\cdot\sqrt{\frac{E_2}{E_1}}\cdot\frac{u_1+u_2}{\Lambda(\vartheta)}, \tag{7}$$

which generalizes the Flamant solution, eqn. (1). Here u_1 and u_2 are the roots of the equation

$$\frac{E_2}{E_1}\cdot u^4 + \left(2\,\nu_{12}\cdot\frac{E_2}{E_1} - \frac{E_2}{\mu_{12}}\right)\cdot u^2 + 1 = 0, \tag{8}$$

and

$$\Lambda(\vartheta) = \frac{E_2}{E_1}\cdot\sin^4\vartheta - \left(2\,\nu_{12}\cdot\frac{E_2}{E_1} - \frac{E_2}{\mu_{12}}\right)\cdot\sin^2\vartheta\cos^2\vartheta + \cos^4\vartheta = \det\left[\mathbf{A}(\vartheta)\right]\cdot\frac{1-\nu_{12}\nu_{21}}{\mu_{12}E_1}, \tag{9}$$

[3] More precisely, this material should be considered elastoplastic, rather than elastic, in conditions where both an elastic or an elastoplastic strain increment may occur. However, the plastic branch of such an elastoplastic material can be analyzed employing an 'elastic comparison material', following concepts introduced by Bigoni and Capuani (2002; 2005). Therefore, the analysis is reduced again to the analysis of the behaviour of an elastic orthotropic

is a quantity proportional to the determinant of the so-called 'acoustic tensor' **A**(ϑ) (Rice, 1977). Therefore, the differential equations governing equilibrium remain (strongly) elliptic until this determinant is strictly greater than zero. Our masonry structure is characterized by a low value of shear modulus μ_{12} and of elastic modulus E_1, the latter particularly in the case of thick joints between bricks. Moreover, the two Poisson's ratios are certainly small and, as a first approximation, they can be taken to be zero, $\nu_{12} = \nu_{21} = 0$, so that the function (9) becomes:

$$\Lambda(\vartheta) = \frac{1}{\mu_{12} E_1}\left(\mu_{12} E_2 \sin^4\vartheta + E_1 E_2 \sin^2\vartheta\cos^2\vartheta + \mu_{12} E_1 \cos^4\vartheta\right). \tag{10}$$

The analysis of the singularity of the acoustic tensor when an elastic modulus tends to zero provides the key to the understanding of localization of deformation (Rice, 1977). The following two cases are of interest to describe our experimental results.

i.) Coefficient μ_{12} tends to zero, while E_1 remains finite. Two shear bands form: one vertical and one horizontal, corresponding to a band normal inclined at $\vartheta = 0$ and $\vartheta = \pi/2$ in eqn. (10) and a shear deformation mode within the band.

ii.) Both E_1 and μ_{12} tend to zero. One vertical compaction/separation band becomes possible, corresponding to a band normal inclined at $\vartheta = 0$ in eqn. (10) and a uniaxial strain deformation mode within the band.

Since in both of the above cases one vertical shear band is always possible, the application of a vertical load will result in a stress map elongated and focussed in the vertical direction. This becomes evident from the analysis reported below.

Solution (7) depends on two independent elastic constants only and, when a uniform load p is applied on a segment of length $2b$, its integration provides a generalization of solution (2) in the form

$$\sigma_{11}(x_1,x_2) = -\frac{p}{\pi}\cdot\sqrt{\frac{E_2}{E_1}}\cdot(u_1+u_2)\int_{-b}^{b}\frac{1}{\Lambda(x_1,x_2,\xi)}\cdot\frac{(x_1-\xi)^2 x_2}{\left[(x_1-\xi)^2+x_2^2\right]^2}d\xi\,,$$

$$\sigma_{22}(x_1,x_2) = -\frac{p}{\pi}\cdot\sqrt{\frac{E_2}{E_1}}\cdot(u_1+u_2)\int_{-b}^{b}\frac{1}{\Lambda(x_1,x_2,\xi)}\cdot\frac{x_2^3}{\left[(x_1-\xi)^2+x_2^2\right]^2}d\xi\,, \tag{11}$$

$$\sigma_{12}(x_1,x_2) = -\frac{p}{\pi}\cdot\sqrt{\frac{E_2}{E_1}}\cdot(u_1+u_2)\int_{-b}^{b}\frac{1}{\Lambda(x_1,x_2,\xi)}\cdot\frac{(x_1-\xi)x_2^2}{\left[(x_1-\xi)^2+x_2^2\right]^2}d\xi\,,$$

where

material.

$$\Lambda(x_1, x_2, \xi) = \frac{1}{\left[(x_1 - \xi)^2 + x_2^2\right]^2}\left[\frac{E_2}{E_1}\cdot(x_1 - \xi)^4 - \left(2\,\nu_{12}\cdot\frac{E_2}{E_1} - \frac{E_2}{\mu_{12}}\right)(x_1 - \xi)^2 x_2^2 + x_2^4\right]. \quad (12)$$

Equations (1) and (7) are exact. However, in the case (i.) of extreme contrast in orthotropy, there is an asymptotic solution available, which approximates eqn. (7). This has been found by Everstine and Pipkin (1971) [4] (see also Christiansen, 1979) and is expressed by

$$\sigma_{11}(x_1, x_2) = 0\,, \qquad \sigma_{2i}(x_1, x_2) = \sigma_{i2}(x_1, x_2) = -\frac{F}{\varepsilon\,\pi}\cdot\frac{x_i}{\left(\frac{x_1}{\varepsilon}\right)^2 + x_2^2}\,, \quad (13)$$

where $i \in [1,2]$ and ε^2 is in our case (in which $\nu_{12} = \nu_{21} = 0$) the ratio between the shear modulus μ_{12} and the vertical elastic modulus E_2. When a uniformly distributed load p acts on a half space, eqn. (13) can be integrated to obtain the following approximation to eqn. (11)

$$\sigma_{11}(x_1, x_2) = 0\,, \qquad \sigma_{2i}(x_1, x_2) = \sigma_{i2}(x_1, x_2) = -\frac{p}{\varepsilon\,\pi}\int_{-b}^{b}\frac{x_i - \xi\,\delta_{1i}}{x_2^2 + \left(\frac{x_1 - \xi}{\varepsilon}\right)^2}d\xi\,, \quad (14)$$

where $i \in [1,2]$ and δ_{1i} is the Kroenecker delta.

The use of eqn. (11) or eqn. (14) is equivalent to our purposes, since results are *qualitatively* identical in both the limit cases (i.) and (ii.) of extreme orthotropy. Hence, maps of in-plane principal stress difference have been plotted in Fig. 6, obtained with eqns. (11) and elastic constants ranging from the isotropic case (Fig. 6a) to the extreme orthotropy where both E_1 and μ_{12} tend to zero (Fig. 6d), keeping $E_1/\mu_{12} = 2$. In particular, Figs. 6b, 6c, and 6d correspond to E_1/E_2 taken equal to 2/3, 1/3, and 1/300, respectively.

An inspection of Fig. 6 clearly reveals that the stress distribution strongly localizes and focusses parallel to the direction of the load when the orthotropy becomes higher, which explains the nearly vertical stress percolation in the masonry models. This finding is in complete agreement with results obtained in elastic solids prestressed near the elliptic boundary by Bigoni and Capuani (2002; 2005); Bigoni and Dal Corso (2008); Bigoni et al. (2007); Dal Corso et al. (2007); Piccolroaz et al. (2006). Therefore, our physical models provide examples of a material characterized by constitutive equations with an extreme orthotropy and therefore near the elliptic boundary, or –in other words– near material instability. Perturbed with concentrated forces, the response of such a material can be interpreted within the theory proposed by Bigoni and Capuani

[4] Everstine and Pipkin (1971) also noticed a 'stress channeling effect' for fiber-reinforced materials, essentially similar to the stress percolation found in our models.

(2002; 2005). [5] Accordingly, the mechanical response is highly localized, so that the stress percolates in a 'narrow channel' almost coaxial with the concentrated force.

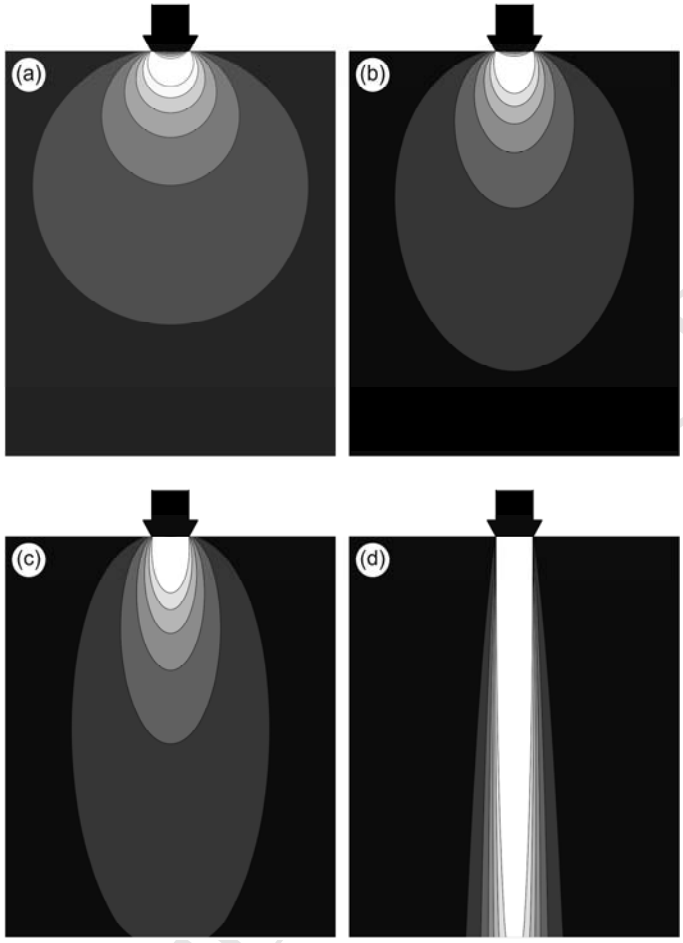

Fig. 6 – Level sets of in-plane principal stress difference for a vertical uniform force (denoted with a thick black arrow) distribution on an area of finite length on an elastic half space, eqns. (9). (a) the isotropic solution; (b) and (c) 'intermediate' values of orthotropy; (d) the highly orthotropic solution, obtained with both E_1 and μ_{12} tending to zero (while $E_1/\mu_{12} = 2$) evidencing nearly vertical stress percolation.

Note that Fig. 6d closely resembles the wave-like stress diffusion pursued by Goldenberg and Goldhirsh (2005), see also Luding (2005) to explain the behaviour of granular materials. [6] In the case (i.) of extreme orthotropy, where only μ_{12} tends to zero, eqns. (14) yields, for $\varepsilon = 1/25$, a plot of the principal in-plane stress difference qualitatively identical to Fig. 5d and therefore the experimental results are fully explained in both cases (i.) and (ii.) of extreme orthotropy.

The solution relative to an extreme orthotropy contrast (Fig. 6d) fully explains the near

[5] The perturbative approach has been recently employed to explain fundamental features of shear band propagation by Bigoni and Dal Corso (2008).

[6] Piccolroaz et al. (2006) have pointed out that the perturbative approach by Bigoni and Capuani (2002; 2005) can be generalized to model the behaviour of granular materials.

vertical stress percolation found in our experiments. The localized stress distribution obtained for high orthotropy contrast degenerates *at* the boundary of ellipticity into a set of vertical lines, transmitting the load without diffusion, as pointed out by Di Pasquale (1992), with reference to the so-called 'no-tension material model' introduced by Heyman (1966).

It should be noted that, consistently with the continuum mechanics assumption and differently from the micromechanics approach, the diversity of stress states within the same masonry structure cannot be now reproduced, since masonry is interpreted as a homogeneous material, while the different localized stress streams are manifestations of the same localized response, differing only for the presence of structural imperfections. A way for reproducing stress-state diversity within a masonry might be pursued by introducing some form of randomly distributed defects in the continuum material, similarly to the randomly distributed dislocations in the simulations of crystal plasticity (van der Giessen and Needleman, 1995), but this leads us beyond the scope of the present investigation.

4. Conclusions

Models of dry masonry walls have been shown to represent: (i.) from micromechanical point of view, an example of a microstructure dominated by random (but constrained within a regular fabric) contacts between bricks; (ii.) from continuum modelling point of view, an example of a material an the verge of an instability. These two points of views have been successfully translated into modelling using micromechanical considerations and the perturbative approach proposed by Bigoni and Capuani (2002); 2005). These models explain experimental results presented in Part I of the present article and open a new perspective in the modelling of masonry structures.

Acknowledgements

The authors gratefully acknowledge financial support from PRIN Grant No. 2007YZ3B24 'Multiscale Problems with Complex Interactions in Structural Engineering' financed by the Italian Ministry of University and Research.

Appendix A. Micromechanical model for thick joints

In a microstructural modelling, we can take into account that the distribution of the contact points between bricks is random, but localized near the edges of the bricks. Roughly speaking, the idea here is to treat every brick as a doubly supported beam by randomly distributed reaction forces (R_1–R_4, to be selected between the three possibilities shown in Fig. 7b), subject to the

vertical loads (F_1–F_4, Fig. 7b) transmitted by the two bricks in the upper course. Note that we have excluded the possibility, never observed in our experiments, that a brick be supported simultaneously at the two edges of the lower bricks. The result of the procedure is a form of random cascade admitting random coalescence, in addition to random branching (Fig. 7 c and d). Note that the width of the bricks is b and the thickness of the joints is d in Fig. 7, so that the reaction forces are determined as

$$\begin{aligned} R_1 &= F_1 + F_2\left(\frac{b+d}{2b}\right) + F_3\left(\frac{b-d}{2b}\right), \\ R_2 &= R_3 = 0, \\ R_4 &= F_4 + F_2\left(\frac{b-d}{2b}\right) + F_3\left(\frac{b+d}{2b}\right) \end{aligned} \tag{15}$$

for mechanism 1; as

$$\begin{aligned} R_1 &= \frac{\langle b(F_1 - F_4) - d(F_1 + 2F_3 + F_4)\rangle}{b-d}, \\ R_2 &= F_1 + F_2 + F_3 + F_4 - R_1 - R_4, \quad R_3 = 0, \\ R_4 &= \frac{\langle b(F_4 - F_1) + d(F_1 + 2F_3 + F_4)\rangle}{b+d} \end{aligned} \tag{16}$$

mechanism 2, and as

$$\begin{aligned} R_1 &= \frac{\langle b(F_1 - F_4) + d(F_1 + 2F_2 + F_4)\rangle}{b+d}, \\ R_2 &= 0, \quad R_3 = F_1 + F_2 + F_3 + F_4 - R_1 - R_4, \\ R_4 &= \frac{\langle b(F_4 - F_1) - d(F_1 + 2F_2 + F_4)\rangle}{b-d} \end{aligned} \tag{17}$$

for mechanism 3.

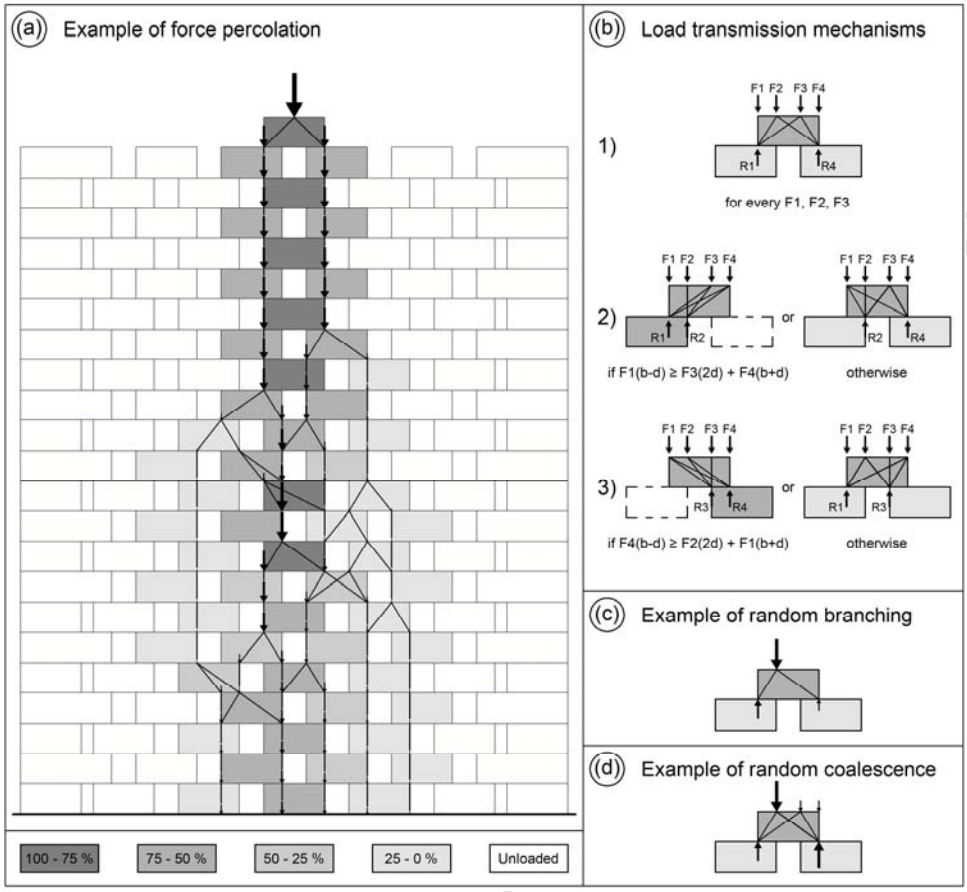

Fig. 7 – Model of a masonry with thick vertical joints as a discrete system with a form of random cascade vertical force transmission, where 'random coalescence' is possible, in addition to random branching. A dark color denotes a high force transmission, so that white bricks are unloaded (see the scale reported in the lower part of the figure, where the transmitted percent of vertical load is reported). (a) a force percolation trees obtained with the model; (b) force splitting-rules for a masonry with thick joints.

We can note from Fig. 4 and Fig. 7 that the proposed micromechanical model correctly reproduces both the tree-like form of the stress percolation and the diversity of 'stress streams' occurring even in nominally identical masonries.

References

Bigoni, D. and Capuani, D. (2002) Green's function for incremental nonlinear elasticity: shear bands and boundary integral formulation. *J. Mech. Physics Solids* 50, 471-500.

Bigoni, D. and Capuani, D. (2005) Time-harmonic Green's function and boundary integral formulation for incremental nonlinear elasticity: dynamics of wave patterns and shear bands. *J. Mech. Physics Solids* 53, 1163-1187.

Bigoni, D. and Dal Corso, F. (2008) The unrestrainable growth of a shear band in a prestressed material *Proc. Royal Soc. A*, 464, 2365-2390.

Bigoni, D., Dal Corso, F. and Gei, M. (2008) The stress concentration near a rigid line inclusion

in a prestressed, elastic material. Part II Implications on shear band nucleation, growth and energy release rate. *J. Mech. Phys. Solids*, 56, 839–857.

Christiansen, R.M. (1979) *Mechanics of composite materials*. Wiley, New York.

Da Silva, M. and Rajchenbach, J. (2000) Stress transmission through a model system of cohesionless elastic grains. *Nature* 406, 708-710.

Dal Corso, F., Bigoni, D. and Gei, M. (2008) The stress concentration near a rigid line inclusion in a prestressed, elastic material. Part I Full-field solution and asymptotics. *J. Mech. Physics Solids* 56, 815–838.

Dal Corso, F., Bigoni, D. and Gei, M. (2008) The stress concentration near a rigid line inclusion in a prestressed, elastic material. Part II Implications on shear band nucleation, growth and energy release rate. *J. Mech. Physics Solids* 56, 839–857.

Di Pasquale, S. (1992) New trends in the analysis of masonry structures. *Meccanica* 27, 173-184.

Everstine, G.C. and Pipkin, A.C. (1971) Stress channelling in transversely isotropic elastic composites. *ZAMP* 22, 825-834.

van der Giessen, E. and Needleman, A. (1995) Discrete dislocation plasticity: a simple planar model. *Modell. Simul. Mater. Sci. Eng.* 3, 689-735.

Goldenberg, C. and Goldhirsh, I. (2005) Friction enhances elasticity in granular solids. *Nature* 435, 188-191.

Johnson, K.L. (1985) *Contact Mechanics*. Cambridge University Press.

Heyman, J. (1966) The stone skeleton. *Int. J. Solids Struct.* 2, 249-279.

Lekhnitskii, S.G. (1981) *Theory of Elasticity of an Anisotropic Body*. Mir Publisher, Moscow.

Luding, S. (2005) Information propagation. *Nature* 435, 159-160.

Piccolroaz, A., Bigoni, D. and Willis, J.R. (2006) A dynamical interpretation of flutter instability in a continuous medium. *J. Mech. Phys. Solids*, 54, 2391-2417.

Rice, J. R. (1977) The localization of plastic deformation. In Koiter, W.T., ed., *Theoretical and Applied Mechanics*. Amsterdam, North-Holland. 207-220.

Liu, C.-h., Nagel, R., Schecter, D.A., Coppersmith, S.N., Majumdar, S., Narayan, O. and Witten, T.A. (1995) Force fluctuation in bead packs. *Science*, 269, 513-515.

Coppersmith, S.N., Liu, C.-h., S.N., Majumdar, Narayan, O. and Witten, T.A. (1996) Model for force fluctuations in bead packs. *Physical Review E*, 53, 4673-4685.

Socolar, J.E.S. (1998) Average stresses and force fluctuations in noncohesive granular materials. *Physical Review E*, 57, 3204-3215.